Disorder and optical gaps in strained dense amorphous carbon and diamond nanocomposites

2012 J. Phys.: Condens. Matter 24 205502

(http://iopscience.iop.org/0953-8984/24/20/205502)

IOP PUBLISHING JOURNAL OF PHYSICS: CONDENSED MATTER

J. Phys.: Condens. Matter **24** (2012) 205502 (8pp) doi:10.1088/0953-8984/24/20/205502

Disorder and optical gaps in strained dense amorphous carbon and diamond nanocomposites

Christos Mathioudakis[1] **and Maria Fyta**[2,3]

[1] Department of Materials Science and Technology, University of Crete, PO Box 2208, 71003 Heraklion, Crete, Greece
[2] Physics Department (T37), Technical University of Munich, 85748 Garching, Germany
[3] Institute for Computational Physics, University of Stuttgart, 70569 Stuttgart, Germany

E-mail: chrm@materials.uoc.gr and mfyta@tum.de

Received 12 October 2011, in final form 1 March 2012
Published 24 April 2012
Online at stacks.iop.org/JPhysCM/24/205502

Abstract

We employ empirical tight-binding simulations on strained tetrahedral amorphous carbon and diamond nanocomposite networks. For each applied strain, the optoelectronic properties are monitored through the absorption coefficient and the dielectric function. These lead to the optical gaps and are able to quantify the amount of disorder in the structures. We compare our results to those of unstrained nanostructured diamond and amorphous carbon (a-C) phases and link the degree of disorder in these materials to their structural details as a function of the external load. The atomic rearrangements and distortions imposed by the external strain in these structures are directly observable in their optoelectronic properties. We thoroughly discuss the interplay between increased external strain, structural and topological disorder, atomic rearrangements and their effect on the calculated optoelectronic properties.

(Some figures may appear in colour only in the online journal)

1. Introduction

The exceptional behavior of carbon in undertaking different kinds of hybridizations to form a variety of interesting structures is widely known. The variability of the existing carbon structures is directly correlated to the majority of applications these can be used for. One of the carbon forms that has been intensively studied is amorphous carbon (a-C), and especially tetrahedral carbon (ta-C), a dense amorphous network which contains a high fraction of sp^3 hybrids [1, 2]. Recently, nanocomposite carbon, which is a more complex structure that includes a crystalline core surrounded by an amorphous carbon matrix has also attracted attention [3]. This composite is also expected to have interesting properties that could possibly be tailored. Specifically, by choosing the type and size of the embedded crystal, as well as the amorphous matrix density, one could obtain a composite material with desired optoelectronic and mechanical properties. Choosing a diamond grain as an inclusion gives rise to diamond nanocomposites (nD/a-C). This is a material which, depending on its density, can have elastic moduli or optoelectronic properties comparable to those of diamond [4, 5]. Dense amorphous networks also show high rigidity and diamond-like optoelectronic properties [1, 6, 7]. In this respect, the ability to tune the properties of diamond nanocomposites and dense amorphous networks reveals a high potential for use in important nanotechnological applications. These can be, for example, hard and wear resistant coatings [8, 9] with hardness and thermal stability comparable to that of diamond. In principle, nanodiamonds and ta-C are biocompatible, and thus potentially suitable for biomedical applications [10]. Nanostructured carbon materials are also expected to lead to applications in MEMS (microelectromechanical devices).

Production of amorphous and nanostructured carbon materials has already been achieved through various methods. Amorphous carbon can be synthesized by various deposition techniques including ion-beam or arc deposition, laser

ablation, ion sputtering and plasma methods [11–14]. The different growth techniques can lead to a variety of a-C networks. These differ in density and sp^3 fraction. The sp^3 fraction can be determined by the equilibrium between densification and relaxation during the growth process [15]. Tuning the desired amorphous network can be achieved by properly selecting the carbon ion energy in the bombardment methods, as well as the substrate temperature [16]. Methods which include some kind of filtering are most commonly used for industrial applications to produce high quality ta-C. These include mass-selected ion-beam deposition (MSIBD) [17] and filtered cathodic vacuum arc (FCVA) methods [18]. Diamond composites, on the other hand, have been grown in both hydrogenated [19] and hydrogen-free [16] a-C matrices. This is achieved by bombardment of highly energetic carbon ions with or without hydrogen species. In a hydrogen-free environment, diamond nucleation can occur by precipitation of small diamond clusters in a dense amorphous network.

The relative ratio of the sp^2 and sp^3 hybrids in both amorphous and diamond nanocomposite materials, their spatial distribution, as well as the size of the diamond inclusion in the latter structures, control the optoelectronic properties of the materials. Such a control would be desirable for potential applications, as already mentioned. However, the use of carbon materials in nanotechnological applications, as mentioned above, poses another problem, that of their stability. Specifically, these materials may operate in conditions in which, for example, high loads are applied. It is thus often desirable to check how the material properties are affected when these operate in various off-equilibrium conditions. In this work we therefore aim to investigate how the properties of two forms of carbon, namely ta-C and dense nD/a-C, can be affected by an external load. We monitor the optoelectronic properties of these two materials as a function of strain. We will focus on the optical gaps and the Urbach energy (E_U), the former being a measure of disorder of the system. We aim to present a systematic study of how tensile strain, as an example of possible external load during operation, affects the equilibrium optoelectronic properties of both ta-C and nD/a-C.

Our work is based on empirical tight-binding molecular dynamics simulations of these structures under strain. The investigation will mainly involve the optoelectronic properties under strain as a probe for the topological and structural disorder in the microstructure. This paper will be structured as follows: in section 2 we discuss the methodology that has been used for structure generation and the calculation of the optoelectronic properties, we then move on to the discussion of the results in section 3 and conclude in section 4.

2. Methodology

The results presented in this work are obtained through tight-binding molecular dynamics (TBMD) simulations. Such a method is appropriate for the problem of nanostructured carbon under strain. First, it is based on a quantum mechanical description of the interactions, being more accurate than empirical schemes. Second, it allows the use of large computational cells compared to the more accurate *ab initio* methods. Specifically, in the case of the nanocomposites, a greater statistical precision through the use of large cells of a few hundred atoms is mandatory and allows for a better description of both amorphous and crystalline phases.

The TBMD method chosen was developed at the Naval Research Laboratory (NRL) [20]. This scheme includes a non-orthogonal model. For the transferability between different structures it uses distance- and environment-dependent parameters. The on-site terms are assumed to be diagonal and sensitive to the environment. The two-center approximation is taken and the hopping integrals depend only on the angular momentum dependence of the orbitals and the distance between the atoms. The scheme concentrates on fitting the Slater–Koster tight-binding parameters to the band structure of the ground state of each material. The equation of state, elastic constants, and phonon frequencies are reproduced for various materials, including carbon structures, while vacancy formation, surfaces, stacking faults, and ductility are also well descried by this TB scheme. Regarding the application of the NRL scheme to carbon structures, the sp parameters for C were obtained by fitting to first-principles results for the band structure and electronic energies of the C_2 dimer, as well as the diamond, graphite, fcc, bcc, and sc forms. The band structure is fitted well and allows for the transferability of the parameters in the amorphous case as well. The NRL scheme gives a good description of the quantum mechanical effects, like the bond breaking studied here, as the fitting was extended to a nearest neighbors distance of about 6.6 ÅThis approach has already been used in similar studies [4]. The density of diamond is calculated at 3.65 g cm^{-3} compared to the experimental value of 3.51 g cm^{-3}. The phonon frequencies are close to the respective experimental data. The trends in the elastic moduli of diamond are also similar to the experimental data, while tensile and shear ideal strengths are also well reproduced [4]. The optoelectronic gap of diamond is ∼5 eV with the present NRL model compared to the experimental value of 5.5 eV. Additional details of the NRL scheme can be found elsewhere [21].

2.1. Structure generation

The ta-C and nD/a-C structures are modeled through computational supercells of 216 and 512 atoms, respectively. Periodic boundary conditions are applied to ensure that the bulk nature of both materials is correctly described. The pure a-C structures are generated by melting a diamond structure and subsequently quenching the melt at constant volume in a canonical (N, V, T) ensemble. The melting started at 6000 K, while a typical quenching duration and rate are 40 ps and 300 K ps^{-1}, respectively. It has been previously shown that different quenching rates, such as 226 and 500 K ps^{-1} do not lead to noticeable differences in the resulting structures [22]. After quenching, the whole material becomes amorphous and both atomic positions and volumes are equilibrated at low temperatures. Additional details on the network generation can be found elsewhere [22].

nD/a-C is a nanocomposite with a spherical diamond core which is embedded in an amorphous carbon matrix. Such a diamond nanocomposite is also generated by quenching from the melt, but in this case the positions of the atoms that belong to the diamond inclusion are kept frozen during the melting and quenching phases. In the end, at low temperatures, all atomic positions, crystalline and amorphous, are allowed to relax. Specifically, the computational cells are relaxed first at 300 K and then at 0 K under the (N, P, T) ensemble. In this way, both the volume and the density fluctuations are allowed to relax and the cell density is equilibrated. This involves a complete relaxation of the external forces and stresses applied to the system [23]. The energy of the system was monitored, and after it reached a minimum the structures were still allowed to equilibrate for an additional 10% of the total relaxation steps. The exact details for the generation of diamond composites are given elsewhere [4, 24]. In both a-C and nD/a-C structures, the coordination and density of the amorphous material is controlled by the volume of the computational cell during quenching. Both the a-C and n-D/a-C investigated here were equilibrated with respect to their atomic positions and volume with the TBMD-NRL scheme.

Specifically, in the current investigation we look at a dense diamond nanocomposite and a dense (ta-C) amorphous carbon network. The equilibrium structures prior to the application of strain have the following structural characteristics. (a) The diamond inclusion in the nanocomposite has a diameter of 12.5 Å. Its volume fraction is 31% and the density of the matrix is 3 g cm^{-3} corresponding to a mean coordination of the amorphous matrix of 3.8. (b) The ta-C network has a similar density and sp^3 ratio. Both materials were strained in a series of incremental strains. For the diamond composites, tensile load is applied along the $\langle 111 \rangle$ direction. Having in mind that the easy-slip plane of diamond is the [111] plane, we choose the crystallographic directions to be those of the nanodiamond region in the composite. Since the a-C phases are highly isotropic, all directions of the applied load are equivalent [4]. In the end, for each strain, the atomic positions were fully relaxed with the TBMD-NRL scheme and all properties are calculated at 0 K. We have previously shown that for the two networks used here their fracture mechanism is similar and occurs at a strain of about 0.11–0.12 [4].

2.2. *Calculation of optoelectronic properties*

For the analysis of the optoelectronic properties of diamond composites and amorphous materials under strain, we use a methodology recently reported for the investigation of the optoelectronic properties of equilibrium unstrained amorphous and nanocomposite networks [5]. We briefly discuss this procedure. The electronic structure is first extracted from the simulations and is correlated to the imaginary part (ε_2) of the dielectric function of the structure. The value of ε_2 can be obtained through a sum over all matrix elements corresponding to transitions from an initial occupied (with an eigenvalue E_i) to a final unoccupied (with an eigenvalue E_f) state. Specifically, ε_2 is defined as $\varepsilon_2 = 2nk$, where n and k are the refractive and the extinction coefficients, respectively. In practice, ε_2 is directly correlated to the electronic structure of the material, and can be given by the sum over all initial and final eigenstates: $\varepsilon_2 = \frac{2}{V}(\frac{2\pi\hbar e}{mE})^2 \sum_{\mathrm{i,f}} |\langle \mathrm{f}|\vec{P}|\mathrm{i}\rangle|^2 \delta(E_\mathrm{f} - E_\mathrm{i} - E)$. In this relation, V is the volume of the cell, e, m are the electron charge and mass, respectively, $\vec{P}$ the momentum operator and E the photon energy. The momentum matrix elements are then extracted by the position matrix elements [5]. Knowledge of ε_2, in turn, leads to the absorption coefficient (α). This is calculated from ε_2 through $\alpha(E) = \frac{E\varepsilon_2}{\hbar n c}$, where E is the energy, c is the speed of light, and n is the refractive index, extracted from the real and imaginary parts of the dielectric function [7]. The E_{04} optical gap used as a probe of the properties of the structures studied here is defined as the energy at which $\alpha(E)$ reaches the value 10^4 cm^{-1}. The concept of the Urbach energy (E_U) is used as a link to the structural and topological disorder in a network. This energy is defined as the inverse of the local slope of $\ln[\alpha(E)]$ at a photon energy of $E = E_{03}$, which is the energy for which the absorption coefficient takes the value 10^3 cm^{-1}. E_U then follows the variations of the absorption coefficient deep within the gap through the equation $E_\mathrm{U}^{-1} = \frac{\mathrm{d}\ln[\alpha(E)]}{\mathrm{d}E}|_{E=E_{03}}$.

The method for deriving the optoelectronic properties for the nanostructured carbon networks is quite efficient. As a consistency check the respective values for crystalline diamond as calculated through this scheme and TBMD approaches compared well to the respective experimental data [5, 25]. Diamond has the highest value compared to a-C and nD/a-C, which have lower optical gaps at low densities [5]. The optical gaps in the case of unstrained diamond composites showed a monotonic relation to the sp^3 ratio in the a-C matrix, reaching the corresponding diamond values for an almost 100% sp^3 fraction. Decomposition into the contribution of the matrix and crystalline atoms showed that for the former there is an increase in the optical gap as the matrix becomes denser, while for the latter at moderate and high densities there is no significant variation with the matrix density. The optical gaps for the diamond nanocomposites, determined by the amorphous matrix having a smaller gap than the inclusion, were found within a range of 1 eV from the respective diamond value [5].

The disorder in these networks can be monitored through E_U [5, 7]. It reflects both structural (bond length and bond angle distortions) and topological disorder which is related to the size distributions of chains and clusters of sp^2 and sp^3 atoms in the mixed phase in a-C [1]. Calculation of the Urbach energy revealed that the disorder in the nanocrystal is noticeable through bond length and angle distortions and appears near the crystalline–amorphous matrix interface. In the case of pure unstrained amorphous networks it was previously shown that the denser networks, i.e. those with a higher sp^3 ratio, show less disorder and develop a non-monotonic behavior to the optical gap and the sp^3 content [7]. A reference value for $E_\mathrm{U} = 0$ corresponds to crystalline diamond. In this respect, the further a network deviates from perfect tetrahedral symmetry, the higher its

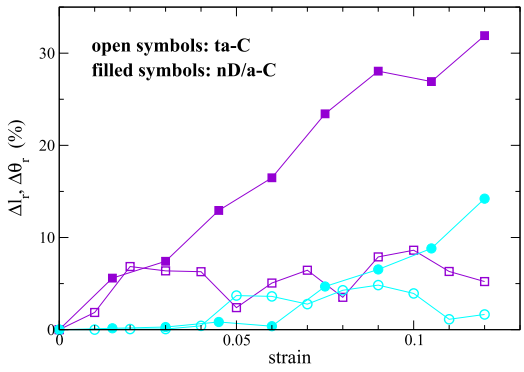

Figure 1. Relative bond length Δl_r (indigo squares) and bond angle $\Delta\theta_r$ (cyan circles) fluctuations as a function of strain ϵ for nD/a-C (filled symbols) and ta-C (open symbols). The absolute values of the fluctuations are shown.

E_U. The highly tetrahedral ta-C network has a high Urbach energy. This is also related to the embedding of minority configurations (sp^2 clusters) into a host majority phase (sp^3 rich network), an effect which produces disorder reflected in the π–$\pi^\star$ subgap transitions.

3. Results and discussion

Following the methodology described in section 2, we have applied tensile strain on a dense amorphous network and a dense diamond nanocomposite. We will first briefly look at the change of the structural characteristics of both networks due to the application of strain ϵ and then discuss the variation of the optoelectronic properties with ϵ and the hybridization ratio.

3.1. Structural characteristics and strain

We first look at the changes in the hybridization content in both networks as strain is increased. In nD/a-C, the initial (strain = 0) sp^2 and sp^3 ratios are 19% and 81%, respectively. Exactly after the fracture point at strain = 0.12, these are 23% and 77%, respectively. The relative values for ta-C at 0 strain are almost the same as for the composite, but at strain = 0.12, the sp^2 (sp^3) fraction is 33% (65%). Hence, the sp^3 ratio in the strained ta-C shows a slightly larger decrease than in the strained nD/a-C (12% instead of 9%). As an additional deeper look into the structural behavior of the networks under load, we also calculated the bond length and bond angle fluctuations as a function of the applied strain ϵ, which are depicted in figure 1. The relative bond length (Δl_r) and bond angle ($\Delta\theta_r$) fluctuations shown in this figure are defined as $\Delta a_r = (\Delta a - \Delta a^0)/\Delta a^0$, where $\Delta a = \sigma_a/\langle a\rangle$ the fluctuations. The superscript 0 corresponds to strain $\epsilon = 0$, which is taken as the reference state. σ_a, $\langle a\rangle$ are the variance and average values of the bond length ($a = l$) or bond angle ($a = \theta$) distributions. In nD/a-C the bond angle distributions are more peaked and less dispersed than the corresponding values for ta-C. The bond length distributions are also slightly more peaked for nD/a-C, but are also as broad as those for ta-C, revealing the variety of different bond lengths in the matrix. For the nanocomposite, the bond and angle fluctuations are in the range 0–32% and 0–15%, respectively. The relevant fluctuations for the amorphous network vary between 0–9% and −5–2%, respectively. The equilibrium values for bond lengths and angles are 1.53 Å and 109.6° for the nanocomposite and 1.52 Å and 109.5° for ta-C, respectively. The a difference between the two strained structures reveals again their different bonding environments. A crude explanation would be that in ta-C the bond lengths and bond angles are already significantly deformed as compared to a highly ordered phase, thus applying external strain will not pose significant rearrangements in the bonding environment. On the other hand, nD/a-C is much more ordered as it contains a crystalline phase and a highly ordered interface with the amorphous matrix. In this respect, strain will impose additional rearrangements in the structural environment of the nanocomposite.

3.2. Dielectric function and absorption coefficient

We begin with the calculation of the imaginary part of the dielectric function in the strained materials. Inspection of ε_2 for the strained ta-C network shows that there is a slight increase of the small shoulder at low energies as the strain increases (data not shown). With increasing strain, the sp^3 ratio decreases. This behavior of ε_2 agrees with the results for unstrained a-C networks with decreasing sp^3 content [26]. However, in the strained amorphous network, the decrease of the four-fold ratio is not that significant, as mentioned above; thus the increase in the small shoulder at low energies in ε_2 is not that pronounced compared to strain $\epsilon = 0$. There is also a slight decrease in the peak of ε_2 in the strained ta-C, which also compares to the variation with decreasing sp^3 content for unstrained a-C [26]. The variation of ε_2 with hybridization ratio for the strained nanocomposites is also similar to the relevant variation in the unstrained composites [5].

We observe in the absorption coefficient for the nanocomposite that the total contribution arises mainly from the contribution of the sp^2 hybrids, i.e. the amorphous matrix atoms which give rise to π–$\pi^\star$ transitions near the energy gap. The variation of the absorption coefficient with energy is shown in figure 2. It is clear that for strained nanodiamonds, but also for ta-C (data not shown), the total absorption coefficient curve shifts towards lower energies as the strain is increased. This is more pronounced for the diamond nanocomposite due to the interface region and the presence of the amorphous matrix. The sp^2 and amorphous (am) contribution shown in the figure follow the total curve closely, revealing that these parts essentially contribute to the total absorption coefficient of the nanocomposite. On the other hand, the sp^3 and diamond core (nD) curves differ from the other contributions, leading to higher optical gaps. The behavior of the different contributions is physically intuitive, since the majority of the sp^3 hybrids reside in the core, while all the sp^2 atoms are in the matrix. For ta-C, the sp^2 contribution also follows the total optical coefficient curve. The total contribution is reflected in the sp^2 part of the

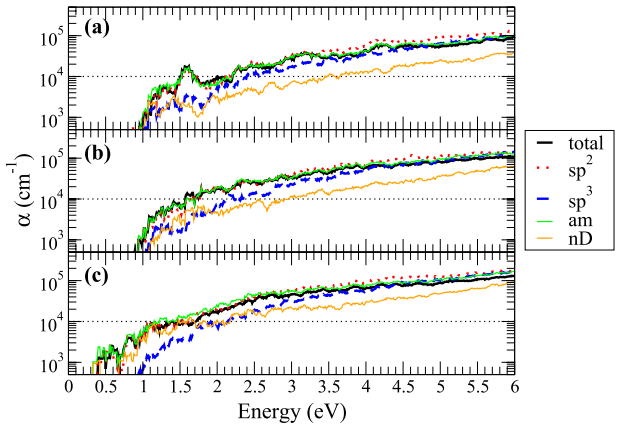

Figure 2. Decomposition of the absorption coefficient α for the diamond nanocomposite at different strains ϵ. The total, sp^2, sp^3, amorphous (am), and core (nD) components of α are represented by the thick-solid (black), red (dotted), blue (dashed), green (solid), and orange (solid) lines, respectively, for (a) $\epsilon = 0$, (b) $\epsilon = 0.06$, and (c) $\epsilon = 0.12$. The black/dotted line corresponds to 10^4 cm^{-1}, which corresponds to the E_{04} optical gap.

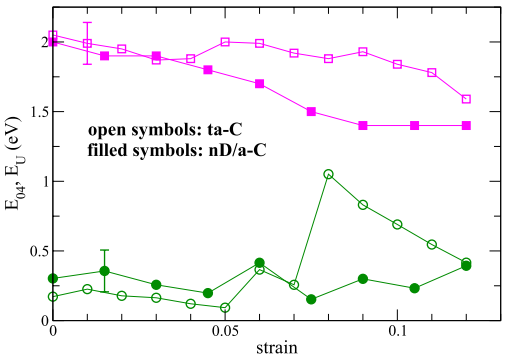

Figure 3. Variation of the optical gap E_{04} (squares) and the Urbach edge E_U (circles) with the applied strain ϵ for nD/a-C (filled symbols) and ta-C (open symbols). One error bar is sketched for each property in order to give an insight into the order of the error in the results. The errors for all the points should be similar, but are not shown for simplicity.

absorption coefficient, in both materials, as the sp^2 hybrids mirror strongly the deviation from tetrahedral symmetry.

3.3. Optical gap, disorder, and strain

Before going into the details of the results, we should note that the errors in the estimation of the optical gap E_{04} and the Urbach energy are of the order of ± 0.15. The estimation was made by accounting for the different approximations that were taken in obtaining the curve for the absorption coefficient α (figure 2) from which the optical gap is calculated, as well as the errors of the fitting to the slope of the absorption coefficient curve, from which the Urbach energy is obtained. These of course include the inherent errors in the TBMD scheme and the calculation of the matrix elements. We next extract the optical gap E_{04} from the absorption coefficient. The variation with strain of the optical gap for the two strained structures, nD/a-C and ta-C, is depicted in figure 3. Both curves consistently decrease as the strain is increased. The maximum difference between the two strained networks is about 0.6 eV and occurs just below the onset of fracture. This is consistent with the larger bond and angle fluctuations at the same strain (see figure 1) 'preparing' the material to break. There is, though, no specific feature at the onset of fracture, around $\epsilon = 0.11$–0.12. In the case of ta-C, a decrease of about 0.6 eV was observed when comparing the material at $\epsilon = 0$ with the fractured one. The respective overall decrease for the nanocomposite is similar (about 0.5 eV). A similar decrease was also evident in E_{04} with a decreasing sp^3 fraction. This decrease was found about 15% higher in the diamond nanocomposite case as compared to ta-C. This is again consistent with the larger bond and angle fluctuations for the same strain in figure 1.

As our next exploration of the disorder in strained nD/a-C and ta-C, we look at the variation of the Urbach edge with the applied strain. The results are shown in figure 3. It is interesting to observe the qualitatively very different behaviors of the two strained structures. For the diamond composite there is no significant variation in the Urbach energy. The values are quite low, between 0.15 and 0.40 eV, without any specific feature close to the onset of fracture (at $\epsilon \sim 0.11$–0.12). In the strained ta-C the variation in the Urbach energy spans a larger energy range from about 0.12 to 1.0 eV, denoting a higher disorder compared to the strained nanocomposite. The additional features in this case are two jumps to higher E_U, denoting higher disorder. This occurs before the onset of fracture in ta-C. Such a feature can probably be attributed to the fact that as the external load is increased there are sudden rearrangements in the material, which lead to elongated and distorted bonds. These deformed bonds are embedded in a majority phase with sp^2 and sp^3 atoms not yet being deformed. This increases the disorder in the network. The structure continues to be strained, the disorder is increased and the Urbach energy increases. At some point, though, the ratio of atoms with elongated (sp^2 or sp^3) bonds becomes significant. The case has now been reversed and the minority phase corresponds to the undistorted bonds. These are embedded in the majority phase of atoms with elongated bonds. In this respect, the disorder and the E_U at this point decreases. The higher E_U values at large strains for ta-C as compared to nD/a-C denote that overall in ta-C the disorder is larger and the clusters of sp^2 atoms, defects and elongated sp^3 atoms define a larger minority phase embedded in the majority phase of the undistorted sp^3 atoms in the materials.

For the case of ta-C, the Urbach energy also follows the non-monotonic behavior (with respect to the four-fold content) of the unstrained non-hydrogenated amorphous networks [7]. Both curves increase abruptly, reach a maximum and then decline less sharply. The difference is that the peak in the Urbach energy is now observed at a strain of about 0.08, which corresponds to about a 75% sp^3 ratio rather than 65% sp^3 in the unstrained amorphous networks [7]. This can be interpreted as a very high disorder half-way before fracture. At that point, the bond rearrangements and

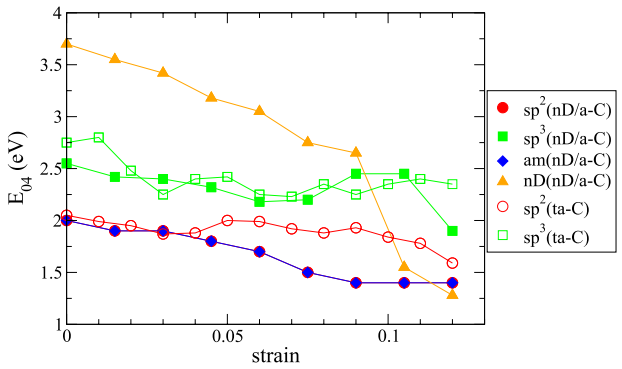

Figure 4. Decompositions into the sp^2, sp^3, amorphous and diamond-core contributions to the optical gap E_{04} in the strained networks. The results are shown as a function of the applied strain ϵ. The sp^2, sp^3, amorphous (am) and diamond-core (nD) contributions are represented by circles, squares, diamonds and triangles, respectively. The open circles and squares correspond to the sp^2, sp^3 contributions for the strained ta-C network and serve as a comparison to the nanocomposite data.

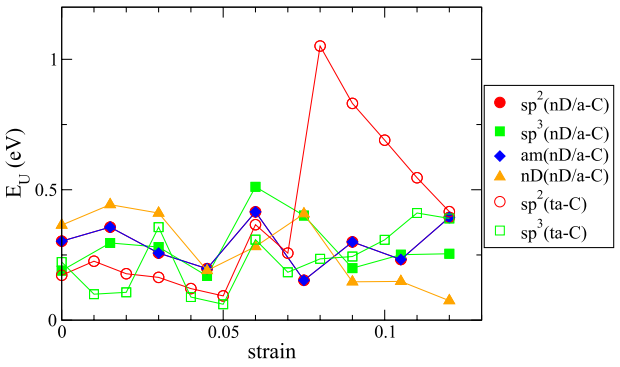

Figure 5. Decompositions into the sp^2, sp^3, amorphous and diamond-core contributions to the Urbach energy E_U in the strained networks. The results are shown as a function of the applied strain ϵ. The sp^2, sp^3, amorphous (am) and diamond-core (nD) contributions are represented by the circles, squares, diamonds and triangles, respectively. The open circles and squares correspond to the sp^2, sp^3 contributions for the strained ta-C network and serve as a comparison to the nanocomposite data.

the relative incompatibilities between the minority phase and the embedding majority phase are larger. In the strained ta-C the amount of disorder 'produced' at a higher sp^3 content is higher. This is evident by the different slopes of the variation with strain around 0.08 ($\sim$75% sp^3) in figure 3, which is compatible to the unstrained amorphous networks [7]. The peak of the E_U distribution with strain is about three times larger in the strained network as compared to the relative variation with the sp^3 content in the unstrained ta-C [7]. Hence, the higher relative disorder in the strained ta-C is again revealed. Note, that at a first glance, the results shown for the Urbach energy in figure 3 do not seem consistent with the relative bond length and angle fluctuations shown in figure 1, as the peak in the E_U does not follow the respective behavior of the bond length and angle fluctuations. Inspection of figure 5, though, shows that the peak in the total E_U is solely attributed to the sp^2 hybrids. In addition to this, we have also checked that at a strain of 0.08, though not mirrored in the overall bond length and angle fluctuations (which include all types of hybrids in the structures), the bond length fluctuations come directly from the three-fold atoms. By this we mean that the sp^2 contribution to the bond length fluctuations coincides with the total fluctuations in the networks at this amount of strain, both contributions showing a sudden drop denoting a higher disorder directly manifested also in the total Urbach energy. Apparently, there is a stronger interplay between minority sp^2 atoms embedded in a four-fold majority phase. These minority sp^2 deformed bonds are embedded in a majority phase with the rest of the atoms not yet deformed. This increases the disorder in the network. The decrease of the Urbach energy at strains larger than 0.08 is related to the overall decrease in the bond length and angle fluctuations in figure 1. We should note here that the peak in the E_U shown in figure 3 at a strain of 0.08 corresponds to an sp^3 ratio of 75% in a very good agreement with figure 4 of [7] and figure 7 of [5], which show the variation of the Urbach energy with the sp^3 fraction for amorphous and diamond nanocomposite networks, respectively. In these figures it is clear that there is an abrupt increase in the E_U at an sp^3 content in the range 65–75%. In this work, similar to these cases, this peak in the Urbach energy has been and is assigned to the argument of 'minority sites embedded in a majority phase' as described above.

We next decompose the optical gap and Urbach edge into contributions from the different hybridizations and the amorphous and crystalline parts in the structure. These results are also compared to relevant data for the strained ta-C and are depicted in figures 4 and 5. First, as evident in both figures, in strained nD/a-C, the sp^2 contribution follows the amorphous one very closely. This is expected, as the sp^2 hybrids are located in the amorphous matrix. The contribution from the sp^3 hybrids resembles more that from the diamond core. This is more strongly expressed in the Urbach energy, revealing that the amount of disorder coming from the distorted sp^3 atoms close to the interface is responsible for the disorder in the diamond core. At the interface, most of the atoms are four-fold with distorted bond lengths as compared to the perfect tetrahedral case. For the optical gap in nD/a-C shown in figure 4 the sp^3 and core contributions do not follow exactly the same trend. The former decreases about 0.6 eV compared to the 2.5 eV decrease of the latter. As strain is applied, the structural rearrangements that are imposed lead to such a deviation from tetrahedral symmetry which moves the optical gap away from perfect tetrahedral symmetry. This is not evident in the relevant decompositions of the Urbach edge in figure 5, since the rearrangements in the core do not correspond to a very high structural difference between an embedding 'minority' and a 'majority' phase.

In ta-C decomposition of the optical gap into its sp^2 and sp^3 contributions shows that the latter follows closely the sp^3 contribution in the nanocomposite, which in turn is dominated by the four-fold atoms in the amorphous matrix (see figure 4). The sp^2 contribution at low strains is similar to that of the nanocomposite, but as the ta-C becomes more strained ($\epsilon >$ 0.05) it is on average about 0.3 eV higher than the respective part in nD/a-C. In the ta-C case, the sp^2 part of the Urbach

energy in figure 5 follows the non-monotonic behavior of the total E_U in figure 3. The high peak in the total E_U in this figure reflects the sp^2 contribution in figure 5. Hence, in the dense amorphous network, the disorder is a result of the structural disorder in the sp^2 hybrids. The disorder in the sp^3 hybrids is lower, as seen in the same figure, and slightly increases at higher loads, where the sp^3 bonds become more elongated.

As a final remark, it is clear so far that for the strained diamond composite larger variations are evident in the optical gaps, while for the strained amorphous network, larger variations are seen in the Urbach energy denoting larger disorder. This can be interpreted through the different mechanisms imposed by the applied strain on these structures. More precisely, in nD/a-C, it was shown that an external load leads to large bond and angle fluctuations. These fluctuations, in turn, are responsible for the larger deviation from tetrahedral symmetry with increasing strain. Due to the high complexity of the structure composed of two phases, amorphous and crystalline, these fluctuations mainly apply to the amorphous phase and the inclusion–matrix interface region. The diamond core is very slightly deformed only at the interface with the matrix. The respective structural rearrangements at the interface and the matrix do not account for as large a structural or topological disorder, through significant structural incompatibilities, as in the case of ta-C. As strain is increased the sp^2 fraction indeed increases, as was shown, but not that significantly. In this sense, the increasing minority sp^2 hybrids within the sp^3 environment are not sufficient to overcome the stronger deviation from perfect tetrahedral symmetry, a deviation that seems more important in the nanocomposite case. On the contrary, in the strained amorphous network, the bond and angle fluctuations are smaller, but the structural incompatibilities that are caused by these fluctuations lead to different geometries and densities within the structure. Increasing the external load leads to more sp^2 hybrids than in nD/a-C. In this respect, there is a stronger interplay between minority sp^2 atoms embedded in a four-fold majority phase, hence larger disorder. Since E_U is a direct measure of the disorder, this is clearly reflected in the amorphous network. Conclusively, in strained nanocomposites the optical gap should be optimally chosen to monitor their structural behavior, while for amorphous networks the Urbach energy would better serve as such a probe.

4. Conclusions

This work includes results based on tight-binding molecular dynamics simulations of strained a-C and diamond nanocomposite structures. Starting from the equilibrium structures we have applied tensile strain along the easy-slip plane of diamond. We have investigated how the optoelectronic properties of the equilibrium structures are affected once strain is applied and compare their properties to those for the unstrained materials. As probes of the optoelectronic properties, we have used the E_{04} optical gap and the Urbach edge. These were decomposed into contributions from the different hybrids in the structures. Our results showed clearly that though the sp^2, sp^3 fractions in all networks did not vary considerably with the applied strain, significant incompatibilities based on the different geometries and densities in the structures occurred. The bond rearrangements due to the external load were directly observed through the decrease of the optical gaps in the strained materials as compared to the unstrained structures. We have also used the concept of the Urbach edge as a measure of the disorder within the strained networks. A more abrupt variation with the applied strain was observed in ta-C, revealing sudden rearrangements in the bonding environment in the materials for certain loads, and thus increased disorder. For the strained nanocomposite, the main finding was that rearrangements in the bonding environment are larger than in strained ta-C. This was not strongly featured in the estimation of the disorder through the Urbach edge, revealing that the bonding rearrangements due to strain are significant, but occur smoothly and lead to significant deviation from the tetrahedral symmetry. The results presented here can serve as a guideline for obtaining information about possible large structural deformations or fracture in amorphous and nanocomposite carbon materials used in nanotechnological applications.

Acknowledgments

MF acknowledges support from the ‘Gender Issue Incentive Funds’ of the Cluster of Excellence in Munich, Germany and the ‘BioFuS’ project of the Intra-European Marie-Curie Actions (call FP7-PEOPLE-2009-IEF). The authors wish to thank I N Remediakis for useful discussions.

References

[1] Robertson J 2002 *Mater. Sci. Eng.* R **37** 129
[2] Silva S R P, Carey J D, Khan R U A, Gerstner E G and Anguita J V 2002 Amorphous carbon thin films *Handbook of Thin Films* vol 4, ed H S Nalwa (New York: Academic) Chapter 9
[3] Lifshitz Y, Kohler T, Frauenheim T, Guzmann I, Hoffman A, Zhang R Q, Zhou X T and Lee S T 2002 *Science* **297** 1531
[4] Fyta M G, Remediakis I N, Kelires P C and Papaconstantopoulos D A 2006 *Phys. Rev. Lett.* **96** 185503
[5] Vantarakis G *et al* 2009 *Phys. Rev.* B **80** 045307
[6] Kelires P C 1994 *Phys. Rev. Lett.* **73** 2460
[7] Mathioudakis C, Kopidakis G, Patsalas P and Kelires P C 2007 *Diamond Relat. Mater.* **16** 1788
[8] Voevodin A A and Zabinski J S 1998 *Diamond Relat. Mater.* **7** 463
[9] Neerinck D, Persoone P, Sercu M, Goel A, Venkatraman C, Kester D, Halter C, Swab P and Bray D 1998 *Thin Solid Films* **317** 402
[10] Chow E K *et al* 2011 *Sci. Transl. Med.* **3** 73
[11] Clausing R E, Horton L L, Angus J C and Koidl P (ed) 1992 *Diamond and Diamond-Like Films and Coatings* (*NATO Science Series B: Physics* vol 266) (New York: Plenum)
[12] Pouch J J and Alterovitz S A (ed) 1990 *Properties and Characterization of Amorphous Carbon Films* (*Mater. Sci. Forum* vol 52/53)
[13] Robertson J 1992 *Surf. Coat. Technol.* **50** 185
[14] Lifshitz Y 1996 *Diamond Relat. Mater.* **5** 388
[15] Lifshitz Y, Kasi S R, Rabalais J W and Eckstein W 1990 *Phys. Rev. B* **41** 10468
[16] Yao Y, Liao M Y, Kohler T, Frauenheim T, Zhang R Q, Wang Z G, Lifshitz Y and Lee S T 2005 *Phys. Rev.* B **72** 035402

[17] Ishikawa J, Takeiri Y, Ogawa K and Takagi T 1987 *J. Appl. Phys.* **61** 2509
[18] Fallon P J *et al* 1993 *Phys. Rev.* B **48** 4777
[19] Lifshitz Y *et al* 2002 *Science* **297** 1531
[20] Cohen R E, Mehl M J and Papaconstantopoulos D A 1994 *Phys. Rev.* B **50** 14694
[21] Papaconstantopoulos D A and Mehl M J 2003 *J. Phys.: Condens. Matter.* **15** R413
[22] Mathioudakis C, Kopidakis G, Kelires P C, Wang C Z and Ho K M 2004 *Phys. Rev.* B **70** 125202
[23] Kelires P C 2000 *Phys. Rev.* B **62** 15686
[24] Fyta M G, Remediakis I N and Kelires P C 2003 *Phys. Rev.* B **67** 035423
[25] Mathioudakis C 2004 unpublished data
[26] Mathioudakis C, Kopidakis G, Kelires P C, Patsalas P, Gioti M and Logothetidis S 2005 *Thin Solid Films* **482** 151